NUCLEATION IN SUPERSATURATED VAPOURS OF SOLID AND LIQUID NAPHTHALENE AND PHTHALIC ANHYDRIDE

Jiří SMOLÍK, Jaroslav VÍTOVEC and Jana VAŠÁKOVÁ

Institute of Chemical Process Fundamentals,
Czechoslovak Academy of Sciences, 165 02 Prague 6-Suchdol

Received September 13th, 1985

The critical supersaturations of vapours of solid naphthalene and phthalic anhydride have been measured by using downward thermal diffusion cloud chamber. The experimental data have been fitted by an empirical fitting formula to allow predictions of behaviour of vapour–non-condesable gas mixtures of both compounds in condensation processes. Including the previously published data on critical supersaturations of vapours, measured above the triple point, the *P-T* diagrams have been drawn for both compounds.

In a recent article[1] we presented the experimental critical supersaturations required for the homogeneous nucleation of naphthalene and phthalic anhydride from their vapours. The experiments were carried out in the temperature range above the triple point of both compounds. Purpose of that article was to determine critical supersaturations as a criterion for prediction of "misting" in hot vapour–gas mixtures during condensation. Since condensation can also take place at the temperatures below the triple point (desublimation) it is desirable to extend existing data to such range of temperatures. Thus the critical supersaturations of vapours of solid naphthalene and phthalic anhydride were measured in a downward thermal diffusion cloud chamber, working in unsteady state. This apparatus and method were tested earlier in stearic acid experiments[2].

EXPERIMENTAL

Experimental procedure and unit. In the downward thermal diffusion cloud chamber, vapour is supersaturated at nonisothermal diffusion flow of substance evaporated from the thin layer of solid on hot top plate and condensed on cooled bottom plate of the chamber. During the operation, the bottom plate is maintained at a constant temperature, while that one of the top plate is increased gradually. Therefore, the supersaturation in the chamber increases until the drops or particles of condensed phase appear. To determine the vapour supersaturation and the temperature for this state, it is necessary to solve the coupled energy and mass transfer equations which describe the mass and energy fluxes between the two chamber surfaces and energy fluxes in both layers of condensate[3]. For these calculations the temperatures of both plates, recorded during the experiment, and the total pressure in the chamber are used.

The chamber used here is identical to the chamber described in previous articles[1,3] with the following exceptions: *a*) the inner surface of the top plate is flat, the plate is heated by contact with special electrical heater with programming of temperature, *b*) the chamber wall is a 26 mm high glass ring, 165 mm i.d. (diameter to height ratio 6·3 : 1) or 21·6 mm high aluminium ring (diameter to height ratio 7·5 : 1) with two glass windows, *c*) the chamber is illuminated by 0·5 mW He–Ne laser.

The temperature of inner surface of the top plate was measured by two NiCr–Ni thermocouples 0·15 mm in diameter. The thermocouples were brought into the chamber through this plate at a point just beside the inner wall and led radially into the center of the plate. The correspondence of measured temperature and actual temperature of the surface during heating was checked by comparison with the melting points of various organic crystals poured over the surface. The uniformity of temperature field of this surface was checked by using liquid crystals. The differences in surface temperature did not exceed 0·3 K in the range of heating rates we used in the individual experiments.

Compounds. The origin, purity and physical properties of the used compounds have been given in the previous study[1]. However, in working with solid compounds, additional physical properties are necessary for experimental data evaluation. Naphthalene vapour pressure[4] $\log P_{eq.} = 11{\cdot}7059 - 2619{\cdot}91/(T - 52{\cdot}499)$ (Pa), thermal conductivity[5] $\lambda = 0{\cdot}7215 - 1{\cdot}25 \cdot 10^{-3} T$ (W m^{-1} K^{-1}), specific heat[6] $c_p = 53{\cdot}43 + 5{\cdot}258T - 8{\cdot}63 \cdot 10^{-3}T^2 + 1{\cdot}55 \cdot 10^{-5}T^3$ (J kg^{-1} . K^{-1}), density[7] $\varrho = 1\,374 - 4{\cdot}64T$ (kg m^{-3}). Phthalic anhydride: vapour pressure[8] $\log P_{eq.} = 14{\cdot}3739 - 4\,632{\cdot}0/T$ (Pa), thermal conductivity[9] $\lambda = -0{\cdot}5244 + 2{\cdot}89 \cdot 10^{-3}T$ (W m^{-1} . K^{-1}), specific heat[6] $c_p = 46{\cdot}17 + 4{\cdot}544\,T - 7{\cdot}46 \cdot 10^{-3}T^2 + 1{\cdot}34 \cdot 10^{-5}T^3$ (J kg^{-1} K^{-1}), density[10] $\varrho = 1\,527$ kg m^{-3}.

RESULTS AND DISCUSSION

Critical supersaturations of vapours of solid naphthalene were measured in the temperature range 230–280 K and of vapours of solid phthalic anhydride in the temperature range 240–300 K. At low concentrations, the particles growing in the chamber were too tiny to be detected reliably and the lower limit was thus given by a visibility of the generating particles. The limiting factors of experiments at higher temperatures were the thickness and quality of the crystalline layer growing on the cold plate. For temperature drop across the layer to be calculated reasonably, it is necessary to have this layer as thin and uniform as possible. However, at higher temperatures, the randomly distributed crystals appeared in the layer of condensate which grew rapidly into the chamber and disturbed the conditions in the chamber during the experiment. Since both effects can influence the experimental results significantly, we shall return to these problems later.

There was an additional effect limiting the experiments with phthalic anhydride. By repeating the same experiment, it was observed that in subsequent run the particles appeared at higher supersaturation. Yet, the particles started to originate at the same supersaturation usually after three runs. The similar effect we observed in the experiments with solid and liquid benzophenone[11]. The results suggest that the heterogeneous nucleation on some foreign particles initiated the preliminary con-

densation. Assuming that the phthalic anhydride is contamined by insoluble foreign particles they can be pushed by the moving solid–melt interface[12] to the inner surface of the solid layer during its preparation and then made free during evaporation. The condensation can start on the largest particles at lower supersaturation initially and on smaller ones at higher supersaturation in the next run. Such size-dependent heterogeneous nucleation has been confirmed experimentally[13]. Once such particles have been removed from the surface layer of the evaporated solid and from the vapour–gas mixture, the same supersaturation is achieved in subsequent runs. This assumption can be supported by the fact that the preliminary condensation was rather insensitive to the increase of supersaturation, but the number density of the particles we observed in subsequent runs increased considerably with slight increase of supersaturation. To eliminate this phenomenon, each experiment was repeated several times until the same supersaturation in subsequent runs was achieved. It was then taken as an experimental result. We did not observe the similar phenomenon in the experiments with naphthalene.

The temperatures of evaporating and condensing surfaces, the rate of heating of the top plate and the total pressure in the chamber, corresponding in the individual experiments to the observed onset of condensation, are given in Table I. The calculated peaks of supersaturation are plotted *versus* temperature in Fig. 1 for naphthalene and in Fig. 2 for phthalic anhydride. In calculation of supersaturation profiles, the existence of solid nuclei was assumed, which can be supposed for the experiments were carried out at the temperatures about 80 K below the triple point of naphthalene and about 130 K below the triple point of phthalic anhydride. Individual curves were fitted by an empirical formula

$$\ln S_{\text{crit.}} = (A - B/T)^{\text{C}} \qquad (1)$$

with parameters given in Figs 1 and 2. The fitting curves (in both Figs denoted by dashed line), which are the envelopes to the individual supersaturation curves, represent the experimental critical supersaturations. A preliminary set of phthalic anhydride experiments had been performed in the chamber with diameter 300 mm two years ago. However, the data exhibited greater scatter probably due to higher surface temperature nonuniformities of considerably greater plate during heating. Yet the data fell very good to the data presented here. It thus confirms the validity of hydrodynamics approximation. To extend the range of temperatures to higher values, the time of duration was shortened by increasing the rate of heating of the top plate by one order of mangitude. To minimalize convection due to differences in the wall and vapour–gas temperatures, the aluminium cylindre wall was used with thermal diffusivity ($\alpha_{\text{Al}} = 0{\cdot}952\ \text{cm}^2\ \text{s}^{-1}$, 350 K[14]) close to thermal diffusivity of helium ($\alpha_{\text{He}} = 1{\cdot}15\ \text{cm}^2\ \text{s}^{-1}$, 350 K, 202 kPa). This method allowed us to extend the temperature range of phthalic anhydride experiments up to 310 K. The data

thus obtained correspond well to the ones presented here. But they exhibited again the greater scatter probably due to temperature nonuniformities at such high heating rates and are not presented here.

Using the individual experimental critical supersaturations determined here and in the previous study[1], the P–T diagrams for naphthalene (Fig. 3) and phthalic anhydride (Fig. 4) were constructed. In both Figs the regions to the right of the curves $P_{eq.}$ represent unsaturated vapour. Along the curves $P_{eq.}$ vapour and solid or liquid co-exist in equilibrium. The regions between curves $P_{eq.}$ and P represent supersaturated vapour, where the rate of nucleation is negligible. If sufficient condensation nuclei or condensation surfaces are not available, the condensation is delayed and the system is in a metastable state. In regions above curves P the rate of nucleation increases rapidly and initiates fog formation. In both Figs P curves are extrapolated and intersect at point B. This point would have simple meaning if the P curves corresponded to homogeneous nucleation in the form of solid or of liquid and both rates of nucleation equaled. Then above this temperature the supersaturated vapour would condense in the form of liquid and below it in the form of solid. With respect to the uncertain mechanism of nucleation in supersaturated

TABLE I

Experimental data: T_1 the temperature of the condensing surface, T_2 the initial temperature of the evaporated surface, T_3 the final temperature of the evaporated surface, r the rate of the heating of the top plate, P the total pressure. The thickness of the evaporated layer in naphthalene experiments was 0·6 mm except for Expts 7, 8, and 11, where the thickness was 1·3 mm. The thickness of the evaporated layer in phthalic anhydride experiments was 0·4 mm

Expt.	T_1, K	T_2, K	T_3, K	r, K min^{-1}	P, kPa
			Naphthalene		
1	228·5	285·1	307·0	2·03	93·6
2	230·0	292·5	309·0	3·40	92·9
3	236·9	291·1	317·8	3·64	94·0
4	237·1	296·6	317·6	3·85	94·7
5	241·1	298·0	320·7	4·13	95·7
6	244·1	289·2	324·2	3·66	94·8
7	246·0	289·2	326·7	3·70	137·7
8	246·1	294·2	327·2	3·93	137·7
9	246·9	293·2	328·0	3·63	97·9
10	247·0	288·5	328·2	3·87	94·8
11	248·2	294·6	330·8	6·14	138·7
12	252·7	290·0	334·9	6·08	97·9
13	254·5	296·1	336·6	6·09	99·2
14	255·7	294·5	338·0	5·81	99·1

TABLE I
(*Continued*)

Expt.	T_1	T_2	T_3	r	P
			Phthalic anhydride		
1	234·0	299·1	302·3	1·45	128·8
2	236·3	302·1	304·8	1·23	132·5
3	236·8	301·5	305·0	1·46	135·5
4	238·1	298·7	307·0	0·75	151·7
5	238·6	300·9	306·7	0·70	153·2
6	241·5	305·3	310·5	0·80	155·6
7	242·4	303·6	310·6	0·61	153·6
8	242·6	304·8	310·6	1·17	155·6
9	245·6	312·1	315·7	0·66	166·4
10	245·9	304·7	316·1	1·44	165·9
11	247·2	305·0	316·8	1·45	157·6
12	247·9	308·8	317·7	1·50	164·1
13	250·0	299·8	319·4	1·56	171·8
14	250·1	310·3	320·1	1·33	168·7
15	250·3	309·3	319·8	1·43	168·3
16	251·1	308·7	320·8	1·54	165·6
17	254·1	313·3	323·1	1·40	167·5
18	254·8	315·7	324·3	1·50	168·7
19	256·5	314·2	325·7	1·54	171·8
20	257·5	314·0	325·5	1·39	172·2
21	260·6	313·6	329·7	1·61	172·5
22	260·8	308·0	329·7	5·45	142·5
23	260·9	314·9	329·8	5·23	143·2
24	260·9	311·8	329·1	5·24	143·9
25	261·3	309·7	329·9	5·64	161·1
26	261·3	307·7	330·3	3·68	160·3
27	261·6	315·1	330·7	1·84	162·3
28	261·8	312·2	330·2	0·76	161·9
29	267·2	318·9	335·3	1·82	163·6
30	267·2	316·4	335·6	3·58	162·9
31	267·9	322·5	335·8	1·66	181·2
32	267·9	323·6	337·1	1·50	181·2
33	276·8	324·1	347·9	5·80	213·0
34	277·0	325·8	348·2	5·29	214·4
35	277·5	323·2	348·6	5·15	170·3
36	277·5	319·5	349·5	5·57	169·2
37	278·6	344·6	350·5	1·19	176·0
38	279·8	333·2	352·0	5·17	211·8
39	279·9	335·8	352·1	5·03	213·0
40	282·5	328·1	354·7	6·02	210·2
41	282·6	331·2	354·9	5·74	210·9

vapours of solids, it rather indicates the range of temperatures of the applicability of individual fitting formulas for prediction of "misting" in supersaturated vapours of both compounds.

The evaluation of experiments comprises the calculation of temperature drop across the layer of condensate growing on the bottom plate. It was like a misty cover at low temperatures, having negligible thickness so that the temperature drop could be neglected. However, at higher temperatures, where the mass flux was considerable, this layer consisted of single crystals growing into the chamber. Thus the layer represented rather porous medium instead of compact one. As the temperature of the bottom plate was constant during the experiments, the only physical property important for the temperature drop calculation was the thermal conductivity of this layer. For porous solids it depends primarily upon geometrical considerations rather than upon the thermal conductivities of solid and gaseous components[15] but it lies somewhere between the thermal conductivities of both components. Thus to estimate an error introduced in calculation of temperature drop across this layer, the thermal conductivity was approximated either by thermal conductivity of compact solid or by that of helium. The calculations were performed for the phthalic anhydride Expts 33–41, assuming the layer thickness 0·1 and 0·3 mm. The differences in surface

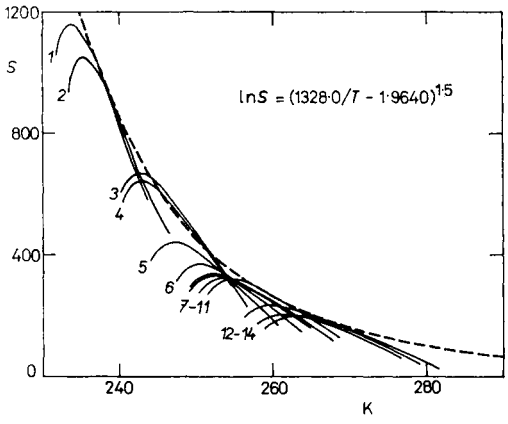

FIG. 1

Variation of the critical supersaturation of naphthalene vapour as a function of temperature. The numbered curves are the solutions of the transport equations for each experiment (Table I). The dashed line, which represents the envelope of the numbered curves, is the experimental result

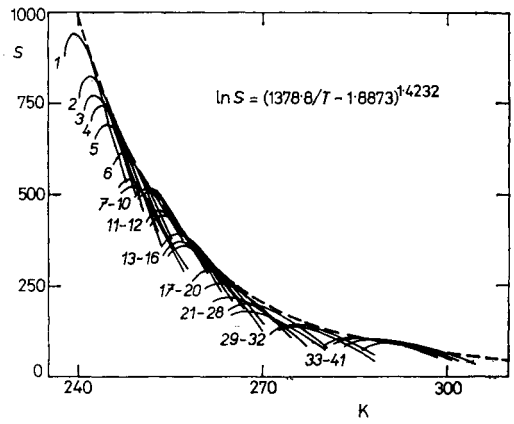

FIG. 2

Variation of the critical supersaturation of phthalic anhydride vapour as a function of temperature. The meaning of the curves as in Fig. 1

temperature were about 0·1 K in the case of 0·1 mm layer, which caused about 2% difference in supersaturation, and about 0·5 K in the case of 0·3 mm layer, resulting in about 6% difference in supersaturation. Thus the error introduced by unknown properties of solid deposit lies in the range of errors of usual cloud chamber studies. To avoid considerable error, the experiments were carried out at the conditions where solid deposit layer did not exceed 0·3 mm. But this requirement did not allow us to extend the temperature range to higher temperatures.

To determine the onset of condensation, particles must grow to a detectable size. Under common conditions the growth phase is of the order of miliseconds and may be neglected. However, when the vapour concentration is sufficiently low, the time for particle to grow to a detectable size can be of the order of seconds[16]. Such long growth times may be important when the experiments are carried out at nonsteady conditions, since supersaturation increases during this growth phase. Thus at low vapour concentrations apparently higher supersaturations may be achieved. To find out whether growth phase had an influence upon the results we presented here, some of phthalic anhydride experiments (Expts 9, 10 and 21–28, see Table I) were repeated, changing the rate of heating only. For Expts 21–28, there was a 5·2% difference in critical supersaturation. Since we did not observe any dependence

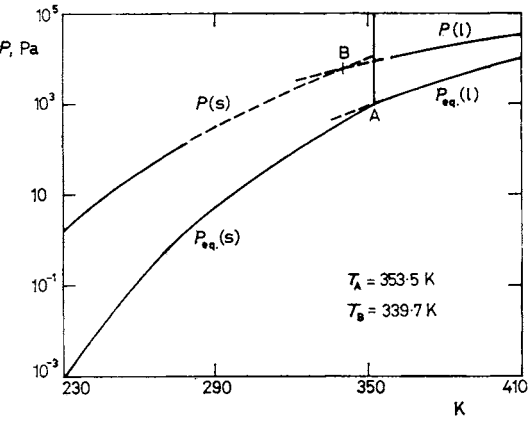

FIG. 3

P–T diagram for naphthalene. $P_{eq.}$ (l) and $P_{eq.}$ (s) are the equilibrium vapour pressures above liquid and solid naphthalene, P(l) and P(s) are vapour pressures for onset of condensation in supersaturated vapour produced by liquid and solid naphthalene. Point A denotes the triple point, point B is the intersection of the extrapolated results

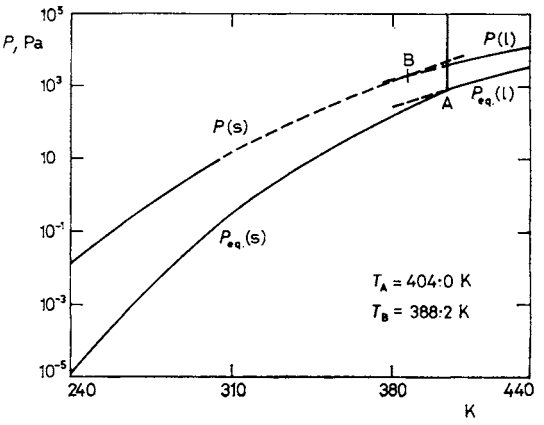

FIG. 4

P–T [diagram for phthalic anhydride. The meanings of curves and points as in Fig. 3

on the rate of heating, the results represent rather the uncertainty inherent in measurements. In Expts 9 and 10 we were not able to discern the influence of different heating rates either. Similar independence on the rate of heating can be deduced from the Expts 1–3 and 4–8. Therefore, the time required for originating particles to grow into the particles large enough to be detected was negligible in these experiments. The onset of condensation was detected by observing the light scattered in the forward direction from the particles originating and growing in the narrow slab of maximum supersaturation. For Mie scattering, the simple conclusions can be drawn from the Mie theory[17]. The intensity of the scattered light is proportional to the intensity of an incident light, it is substantially higher in the forward direction, and the first maximum on intensity curve appears at the diameter of particle comparable with the wavelenght of incident light. Therefore, for intensive monochromatic radiation with wavelength 0·63 μm, produced by He–Ne laser, the particles with the diameter close to this value might be detected.

In order to estimate the size of particles we observed, the rates of growth as well as the settling velocities were calculated by using the procedure given in Appendix. In these calculations we assumed an isothermal growth of spherical particle being in rest under the conditions prevailing at the point of touch of individual supersaturation curves and the envelope. The calculations were carried out for the terminal particle diameters 0·5, 2, and 5 μm. If we neglect variation of vapour–gas viscosity with composition and temperature, the settling velocities of these particles are 0·016, 0·2, and 4·7 mm s^{-1} for all phthalic anhydride experiments. The average time of growth of such particles is 0·4, 2·7, and 13·1 s for Expts 21–28 and 2·0, 13·7, and 66·7 s for Expts 9 and 10. The comparison of calculated values with experiments (independency on heating rate, condensation in narrow slab of maximum supersaturation only and very slow settling velocities we observed) indicates that the diameter of particle we were able to detect lies between 0·5 and 2 μm, *i.e.* close to the wavelenght of light, the particles were enlighted with. At the lowest concentrations (Expt 1), the times of growth of the same particles are 8·3, 55·6, and 266 s, nevertheless, the curve falls to the experimental critical supersaturation curve. It suggests that the particle with the diameter comparable to the wavelength of incident light could be detected. The corresponding supersaturation shift, caused by increasing the supersaturation during the particle growth, was about 2·9% for Expt 1. The inspection to Figs 3 and 4 reveals that the substantially higher vapour concentrations were achieved in naphthalene experiments. Accordingly, the growth of particles has not been analysed.

APPENDIX

We assume an isothermal growth of spherical particle, originating as a critical nucleus in a binary mixture of vapour and gas. Furthermore, we assume that the particle is in rest, that the number

density of vapour molecules n_v is substantially lower than that one of gas molecules $n_g (n_v \ll n_g)$. that the vapour–gas mixture behaves ideally and that the condensation coefficient equals unity,

Then, the growth rate can be calculated according to the set of equations[18,19]

$$\varrho \, \mathrm{d}r/\mathrm{d}t = J \tag{1}$$

$$r_0 = 2\gamma M_v/(\varrho R T \ln (P_v/P_{eq.})) \tag{2}$$

$$J = J_K \, . \, 1{\cdot}333 Kn_v (1 + (1{\cdot}333 Kn_v + 0{\cdot}71)/(1 + Kn_v^{-1}))^{-1} \tag{3}$$

$$J_K = M_v (P_v - P_{v,r})/(2\pi M_v R T)^{1/2} \tag{4}$$

$$P_{v,r} = P_{eq.} \exp (2\gamma M_v/\varrho R T r) \tag{5}$$

$$Kn_v = \lambda_v / r \tag{6}$$

$$\lambda_v = 32 \Omega_{vg}^{(1,1)*}/(3\pi(1 + M_v/M_g)) \, . \, (D_{vg}/\bar{c}_v) \tag{7}$$

$$\bar{c}_v = (8RT/\pi M_v)^{1/2} \tag{8}$$

The Eqs. (*1*) and (*3–8*) with initial condition (*2*) were solved numerically by Euler method.

Settling velocity of particles was calculated by using Stokes equation with Cunningham correction factor[20].

$$v = 2r^2 \varrho g C_c / 9\mu \tag{9}$$

$$C_c = 1 + Kn_g (1{\cdot}257 + 0{\cdot}4 \exp (-1{\cdot}1/Kn_g)) \tag{10}$$

$$Kn_g = \lambda_g / r \tag{11}$$

$$\lambda_g = (\sqrt{2}\pi n_g \sigma_g^2)^{-1} \, , \quad (n_v \ll n_g) \tag{12}$$

$$n_g = P_g / kT \tag{13}$$

LIST OF SYMBOLS

$\bar{c}$	average absolute velocity of the molecule
C_c	Cunningham correction factor
D_{vg}	binary diffusivity
g	acceleration due to gravity
J	mass flux
k	Boltzmann's constant
Kn	Knudsen number
M	molecular mass
n	number density of molecules
P	pressure
r	radius of the particle
R	gas constant
t	time
T	temperature
v	velocity

Greek letters

γ	surface energy
λ	mean free path of the molecule
μ	viscosity
σ	collision diameter
ϱ	density
$\Omega_{vg}^{(1,1)*}$	collision integral

Subscripts

eq.	refers to the equilibrium value
g	refers to the gas
K	refers to the kinetic theory of gases
0	refers to an initial condition
r	refers to the surface of the particle
v	refers to the vapour

REFERENCES

1. Smolík J., Vítovec J.: This Journal *50*, 1349 (1985).
2. Smolík J., Vítovec J.: J. Aerosol Sci. *14*, 697 (1983).
3. Smolík J., Vítovec J.: Int. J. Heat Mass Transfer *26*, 975 (1982).
4. Fowler L., Trump W. N., Vogler C. E.: J. Chem. Eng. Data *13*, 209 (1968).
5. Touloukian Y. S. (Ed.): *Thermophysical Properties of Matter* (*The TRPC Data Series*), Vol. 2, *Thermal Conductivity — Nonmetallic Solids*, p. 997. IFI/Plenum, New York 1970.
6. Landolt–Börnsteins *Zahlenwerte und Funktionen aus Physik-Chemie-Astronomie-Geophysik-Technik*, p. 524, 525. Springer, Berlin 1960.
7. *Beilsteins Handbuch der Organischen Chemie*, Vol. 7. Springer, Berlin 1963.
8. Crooks D. A., Feetham F. M.: J. Chem. Soc. *1946*, 899.
9. Suter H.: *Phthalsäureanhydrid und seine Verwendung*. D. Steinkopf Verlag, Darmstadt 1972.
10. *Kirk–Othmer Encyclopedia of Chemical Technology*, Vol. 15, p. 445. Wiley, New York 1968.
11. Smolík J., Vítovec J.: This Journal *43*, 2664 (1978).
12. Kuo V. H. S., Wilcox W. R.: Ind. Eng. Chem., Process Des. Develop. *12*, 376 (1973).
13. Porstendörfer J., Scheibel H. G., Pohl F. G., Preining O., Reischl G., Wagner P. E.: Aerosol Sci. Technol. *4*, 65 (1985).
14. Touloukian Y. S. (Ed.): *Thermophysical Properties of Matter* (*The TRPC Data Series*) Vol. 10, *Thermal Diffusivity*, p. 2. IFI/Plenum, New York 1973.
15. Satterfield C. N.: *Mass Transfer in Heterogeneous Catalysis*, p. 69. M.I.T. Press, Cambridge 1970.
16. Becker C.: J. Chem. Phys. *72*, 4579 (1980).
17. Van de Hulst H. C.: *Light Scattering by Small Particles*. Wiley, New York 1957.
18. Davis E. J., Ray A. K.: J. Aerosol Sci. *9*, 411 (1978).
19. Davis E. J., Ravindran P., Ray A. K.: Chem. Eng. Commun. *5*, 1 (1980).
20. Reist P. C.: Introduction to Aerosol Science, p. 53. Macmillan, New York 1984.

Translated by the author (J. S.).